ELSEVIER

Comput. Methods Appl. Mech. Engrg. 185 (2000) 1–19

Computer methods in applied mechanics and engineering

www.elsevier.com/locate/cma

A posteriori error estimation for finite-volume solutions of hyperbolic conservation laws

X.D. Zhang *, J.-Y. Trépanier, R. Camarero

Centre de Recherche en Calcul Appliqué (CERCA) and Department of Mechanical Engineering, Ecole Polytechnique de Montréal, 5160 Boulevard Décarie, Bureau 400, Montréal, Québec, Canada, H3X 2H9

Received 18 December 1996; accepted 30 September 1998

Abstract

In this paper, an a posteriori error estimation technique for hyperbolic conservation laws is proposed. The error distributions are obtained by solving a system of equations for the errors which are derived from the linearized hyperbolic conservation laws. The error source term is estimated using the modified equation analysis. Numerical tests for one-dimensional linear and non-linear scalar equations and systems of equations are presented. The results demonstrate that the error estimation technique can correctly predict the location and magnitude of the errors. In addition, it is shown in an example that the estimated error source terms can be used for grid adaptation to control the magnitude of error.

Keywords: Error estimation; Error source; Finite-volume method; Hyperbolic equations

基于残差的自适应算法推导. 较详细

1. Introduction

The use of locally adaptive computational grids is one of the most attractive strategies to achieve highly accurate solutions of partial differential equations. The generation of such adapted grids is usually guided by a proper a posteriori error estimation technique. Such techniques abound for finite-element methods, but for finite-volume methods, the theoretical foundation of a posteriori and a priori error analysis is far from satisfactory. This is especially true for hyperbolic problems [1].

Most error estimation techniques used for grid adaptation in finite-volume methods are based on the local flow structure, which means that the predicted errors are not influenced by distant information (i.e. convection of error is not accounted for). Many widely used error estimators and indicators are based on the local gradient of density or Mach number [2,3]. In these cases, the predicted error may become unbounded with the grid refinement near discontinuities. Alternatives have been proposed based on cell-length adjusted velocity derivatives [4] or on cell-length weighted density gradients [5]. Another strategy using residual as a mesh refinement indicator has been used in Ref. [6] for compressible Euler equations. However, the residual represents the error source, not necessarily the solution error as will be demonstrated in this paper.

In fact, for hyperbolic systems, the errors arising from the numerical discretization act as erroneous waves which are propagated by the equations in the same manner as physical waves. Thus the source of an error may manifest itself far away from its active point. Error indicators based on a local analysis of the solution may produce a misleading error distribution and may not be able to identify the error source.

* Corresponding author.

0045-7825/00/$ - see front matter
PII: S0045-7825(99)00099-7

Solving an appropriate equation for the error may prove to be a more effective and reliable approach to error estimation.

In Ref. [7], an error equation was derived for scalar linear advection–diffusion problems and a discrete residual estimate is used as an error source for the error equation by assuming that the approximated solution is smooth across the interfaces of each control volume. For non-smooth or discontinuous approximation often arising in finite-volume methods, the error source may be modified by accounting for the jump in the solution across the element boundaries, as discussed in Refs. [8,9] in a finite-element context. To the authors' knowledge, very little work has been done for non-linear hyperbolic systems of conservation laws solved using a finite-volume method.

In the present paper, a dynamic procedure for a posteriori error estimation for hyperbolic conservation laws is proposed and tested. This method is based on solving linearized hyperbolic equations for the errors with source terms obtained using the modified equation analysis [10,11]. The dominant term in the modified equation is used as the error source. This provide an alternative way of accurately estimating the solution error for hyperbolic equations. This technique accounts for the wave structure of the solution. In particular it will detect convection of errors which is a non-local phenomena. Also, it will be shown that efficient grid adaptation can be achieved by using the estimated error source instead of the solution error itself. The estimated a posteriori error distribution can be used as a verification of the grid adaptation algorithm. In Sections 2 and 3, the hyperbolic system of conservation laws and the corresponding error equations are presented. Section 4 details the method to estimate the error source term. Numerical experiments for one-dimensional test cases are presented in Section 5.

2. Equations and the finite-volume scheme

In this paper, we consider the following one-dimensional hyperbolic system of conservation laws

$$u_t + [f(u)]_x = 0, \quad x \in \Omega, \ \ t \geqslant 0, \tag{1}$$

where $u = u(x,t)$ is an unknown vector, $f(u)$ the vector-valued flux function of u. For hyperbolic conservation laws, one assumes that the Jacobian matrix

$$A(u) = f_u(u)$$

has only real eigenvalues and can be diagonalized as

$$A(u) = LDR,$$

where $D = \mathrm{diag}(\lambda^1, \lambda^2, \ldots)$ is the diagonal matrix consisting the eigenvalues of A, L and $R(= L^{-1})$ are formed from the left and right eigenvectors of A, respectively.

The explicit time-marching discretization of the integral form of Eq. (1), using the finite-volume scheme with equal spacing Δx, can be written as follows:

$$u_i^{h,n+1} = u_i^{h,n} - \frac{\Delta t}{\Delta x}(f_{i+1/2}^{h,n} - f_{i-1/2}^{h,n}), \tag{2}$$

in which $\Delta t = c\Delta x / \max_{i,j} \lambda_i^j$ is the global time step with a Courant–Friedrichs–Lewy (CFL) number of c. Superscripts h and n represent the finite-volume solution and the time level respectively while subscripts denote space location. The average cell value is defined as

$$u_i^n = \frac{1}{\Delta x} \int_{x_{i-1/2}}^{x_{i+1/2}} u(x, t^n)\, \mathrm{d}x.$$

The interface flux value $f_{i+1/2}^{h,n}$ will differ for different finite-volume schemes. In the present study, Roe's characteristic upwind flux-difference-splitting scheme [12] is used, and the flux is given by

$$f_{i+1/2}^{h,n} = f_R(u_{i+1}^{h,n}, u_i^{h,n}) = \frac{1}{2}(f_{i+1}^{h,n} + f_i^{h,n}) - \frac{1}{2}\left|\Delta f_{i+1/2}^{h,n}\right|, \tag{3}$$

where

$$\left|\Delta f^{h,n}_{i+1/2}\right| = \left|\tilde{A}^{h,n}_{i+1/2}\right|(u^{h,n}_{i+1} - u^{h,n}_{i}), \tag{4}$$

is the upwinding term, and

$$f^{h,n}_i = f(u^{h,n}_i),$$

$$|A| = L|D|R, \tag{5}$$

$$\tilde{A}^{h,n}_{i+1/2} = \tilde{A}(u^{h,n}_{i+1}, u^{h,n}_{i}) = A(\tilde{u}^{h,n}_{i+1/2})$$

in which $|D| = \mathrm{diag}(|\lambda^1|, |\lambda^2|, \ldots)$. The tilde represents Roe's averaged value and, for any two values of u_1 and u_2, the averaged matrix satisfies

$$f(u_1) - f(u_2) = \tilde{A}(u_1, u_2)(u_1 - u_2), \quad \tilde{A}(u_1, u_1) = A(u_1). \tag{6}$$

Details can be found in Ref. [12]. In the case of a single equation, the Jacobian is simply a single-valued function of u_1, and $A = D = \lambda$.

3. Error equation

3.1. Derivation

Consider the hyperbolic system of conservation laws given in Eq. (1) and its finite volume approximation u^h, the following residual can be defined

$$u^h_t + [f(u^h)]_x = r(u^h). \tag{7}$$

Defining the error vector as $\epsilon = u - u^h$, subtracting Eq. (7) from Eq. (1) and using relations given in Eq. (6), it is clear that

$$\epsilon_t + [\tilde{A}(u, u^h)\epsilon]_x = -r(u^h)$$

or

$$\epsilon_t + [\tilde{A}(u^h + \epsilon, u^h)\epsilon]_x = -r(u^h), \tag{8}$$

which is a non-linear equation for the error vector ϵ. In practice, it is reasonable to replace u by u^h in the Jacobian matrix and the above equation becomes

$$\epsilon_t + [A(u^h)\epsilon]_x = -r(u^h). \tag{9}$$

This is a linear hyperbolic system of equations for the error vector with an extra error source given as the negative of the residual $-r(u^h)$.

3.2. Initial and boundary conditions

For initial value problem (IVP), the initial conditions for Eqs. (1) and (9) are quite simple and can be given as

$$u(x, t = 0) = \phi(x),$$
$$\epsilon(x, t = 0) = u - u^h = 0.$$

For IVP with $\Omega = (-\infty, \infty)$, there are no boundary conditions to specify. However, for a boundary value problem (BVP) or an initial-boundary value problem (IBVP) with $\Omega = [a, b]$, boundary conditions

must be specified. In this paper, the boundary conditions are specified in ghost cells by imposing values or extrapolating from internal cells using the local characteristics. For example, the boundary treatment for the error Eq. (9), can be explained in the following procedure:

First, for all boundary cells, the characteristic error variables $R\epsilon$ are computed according to:

$$[R\epsilon]_a^j = \begin{cases} 0 & \text{(analytic)} \quad \text{for } \lambda^j \geqslant 0 \\ [R\epsilon]_{\text{int}}^j & \text{(extrapolate)} \quad \text{otherwise} \end{cases} \tag{10}$$

and

$$[R\epsilon]_b^j = \begin{cases} 0 & \text{(analytic)} \quad \text{for } \lambda^j \leqslant 0, \\ [R\epsilon]_{\text{int}}^j & \text{(extrapolate)} \quad \text{otherwise,} \end{cases} \tag{11}$$

where $[R\epsilon]_{\text{int}}^j$ is the value at the internal neighboring cell.

Then the values for the error variables in the image cells are obtained as:

$$\epsilon_{a,b} = L[R\epsilon]_{a,b},$$

and $[R\epsilon]_a$, $[R\epsilon]_b$ are the boundary values as given in (10) and (11), respectively.

4. Error source approximation

The modified equation approach is used for approximating the error source $-r(u^h)$ for Eq. (9). The idea of using the modified equation analysis to identify and remove the dominant errors for hyperbolic equations can be found in Refs. [10,11]. The modified equation analysis is basically designed for the finite difference scheme using Taylor series expansion based on a set of discrete data. An intrinsic assumption of smooth interpolation between those discrete data is made. To apply this analysis for the present finite-volume scheme to obtain a reasonable error source estimation, one can regard the discretized Eq. (2) as a finite-difference algorithm. Thus the cell-averaged states $u_i^{h,n}$ from the finite-volume scheme will be used as the discrete cell values of the numerical solution $u^h(x,t)$. It is noted that the difference between these two interpretations is of the order $O(\Delta x^2)$ in smooth flow regions.

From Eqs. (2) and (3), and the Taylor series expansion for $u_{i+1}^h, f_{i\pm1}^h$, it is easy to arrive at the following modified equation at grid point i

$$u_t^h + [f(u^h)]_x = \frac{1}{2\Delta x}\left(\left|\Delta f_{i+1/2}^h\right| - \left|\Delta f_{i-1/2}^h\right|\right) - \frac{\Delta t}{2}\frac{\partial^2 u^h}{\partial t^2} - \frac{\Delta x^2}{6}\frac{\partial^3 f^h}{\partial x^3} - \frac{\Delta t^2}{6}\frac{\partial^3 u^h}{\partial t^3} + O\left(\Delta x^3, \Delta t^3\right). \tag{12}$$

The first term on the RHS of the above equation will be used in the residual approximation. However, it can be replaced by the following expression when Taylor series are also used for $u_{i\pm1}^h$ and $|\tilde{A}_{i\pm1}^h|$ from Eq. (4)

$$\frac{1}{2\Delta x}\left(\left|\Delta f_{i+1/2}^h\right| - \left|\Delta f_{i-1/2}^h\right|\right) = \frac{\Delta x}{2}\left(\frac{\partial|\tilde{A}^h|}{\partial x}\frac{\partial u^h}{\partial x} + |\tilde{A}^h|\frac{\partial^2 u^h}{\partial x^2}\right) + O\left(\Delta x^3\right). \tag{13}$$

Retaining only the leading terms and noting that

$$\frac{\partial^2 u^h}{\partial t^2} = \frac{\partial}{\partial x}\left(A^h\frac{\partial f^h}{\partial x}\right) + O(\Delta x, \Delta t),$$

Eq. (12) becomes

$$u_t^h + [f(u^h)]_x = \frac{\Delta x}{2}\left(\frac{\partial|\tilde{A}^h|}{\partial x}\frac{\partial u^h}{\partial x} + |\tilde{A}^h|\frac{\partial^2 u^h}{\partial x^2}\right) - \frac{\Delta x}{2}\frac{\partial}{\partial x}\left(A^h\frac{\partial f^h}{\partial x}\right) + O\left(\Delta x^2, \Delta t^2, \Delta x\Delta t\right), \tag{14}$$

Thus, the error source term is given by

$$-r(u^h) = -\frac{\Delta x}{2}\left(\frac{\partial|\tilde{A}^h|}{\partial x}\frac{\partial u^h}{\partial x} + |\tilde{A}^h|\frac{\partial^2 u^h}{\partial x^2}\right) + \frac{\Delta t}{2}\frac{\partial}{\partial x}\left(A^h\frac{\partial f^h}{\partial x}\right) + O\left(\Delta x^2, \Delta t^2, \Delta x\Delta t\right). \tag{15}$$

For practical computations, the first term on the RHS in Eq. (15) is discretized in the same way as the LHS term in Eq. (13). The second term on the RHS in Eq. (15) is discretized as

$$\begin{aligned}\frac{\Delta t}{2}\frac{\partial}{\partial x}\left(A\frac{\partial f}{\partial x}\right) &\approx \frac{\Delta t}{2\Delta x}\left[\left(A\frac{\partial f}{\partial x}\right)_{i+1/2}-\left(A\frac{\partial f}{\partial x}\right)_{i-1/2}\right]\\ &\approx \frac{\Delta t}{2\Delta x^2}\left[\tilde{A}_{i+1/2}(f_{i+1}-f_i)-\tilde{A}_{i-1/2}(f_i-f_{i-1})\right]\\ &= \frac{c}{2\Delta x \max_{i,j}|\lambda_i^j|}\left[|\tilde{A}_{i+1/2}||\Delta f_{i+1/2}|-|\tilde{A}_{i-1/2}||\Delta f_{i-1/2}|\right],\end{aligned}$$

where $\Delta f = \tilde{A}\Delta u$ from Eq. (6) has been used. Finally, neglecting the higher-order terms leads to

$$-r_i^h \approx -\frac{1}{2\Delta x}\left[\left(I - c\frac{|\tilde{A}^h_{i+1/2}|}{\max_{i,j}|\lambda_i^{h,j}|}\right)|\Delta f^h_{i+1/2}| - \left(I - c\frac{|\tilde{A}^h_{i-1/2}|}{\max_{i,j}|\lambda_i^{h,j}|}\right)\left|\Delta f^h_{i-1/2}\right|\right], \tag{16}$$

where I is the unit matrix. For steady-state problem, all time-derivatives in Eq. (12) vanish, which results in the following expression for the error source:

$$\begin{aligned}-r(u^h) &= -\frac{\Delta x}{2}\left(\frac{\partial|\tilde{A}^h|}{\partial x}\frac{\partial u^h}{\partial x}+|\tilde{A}^h|\frac{\partial^2 u^h}{\partial x^2}\right)+\frac{\Delta x^2}{6}\frac{\partial^3 f^h}{\partial x^3}+\mathrm{O}(\Delta x^3).\\ -r_i^h &\approx -\frac{1}{2\Delta x}\left(\left|\Delta f^h_{i+1/2}\right|-\left|\Delta f^h_{i-1/2}\right|\right).\end{aligned} \tag{17}$$

In these approximations, $|\Delta f^h_{i\pm1/2}|$ is simply the upwinding terms given in Eq. (4). For unsteady cases, the error Eq. (9) should be solved simultaneously with the flow Eq. (1), so as to reuse the upwinding terms. For steady-state computations, the matrix $A(u^h)$ and the error source $-r(u^h)$ are computed only once. Hence the computational cost for their evaluation is negligible.

5. Results and discussion

We now present tests of the previously described procedure for error estimation. Four cases possessing closed form solutions are used:

(i) a linear advection equation,
(ii) a non-linear Burgers' equation,
(iii) the unsteady Euler equations,
(iv) the steady Euler equations with variable cross-section.

It is well known that the first-order upwind scheme is very diffusive. If the diffused solution is fed into the error Eq. (9) and a first-order scheme is used to solve this equation, then the estimated error distribution will be further diffused. In a finite-element context, the need to use a higher order scheme for solving the error equation has been discussed by Pelletier et al. [9]. In the present approach, the error source term for the error equation is of order $\sim \mathrm{O}(\Delta x^k)$ if a kth-order scheme is used for solving Eq. (1). To avoid introducing significant numerical error when solving the error equation, a higher order (say $k+\alpha$ with $\alpha > 0$) scheme is needed to solve the error equation such that the truncation error for discretizing the error equation has at least an order of $\mathrm{O}(\Delta x^{k+\alpha})$. For comparison, both the first-order scheme and the space-time reconstructed second-order scheme [13] are used for solving the error equations while only a first-order scheme is used for the hyperbolic flow equations.

5.1. Linear advection equation

The simple linear problem used by Leonard [14] is considered first. The flux function is the variable itself and the Jacobian is equal to one. This test problem is an unsteady, one-dimensional pure advection IVP. The initial condition consists of three parts: a unit step, a sine-squared wave and a semi-ellipse.

A uniform mesh with spacing $\Delta x = 0.01$ is used for this problem. First, the unit step change in u initially set at $x_1 = 0.1$.

The second profile is an isolated sine-squared wave of width $20\Delta x$ initially started at $x_2 = 0.7$:

$$\phi(x) = \begin{cases} \sin^2\left(\dfrac{\pi(x - x_2)}{20\Delta x}\right) & \text{for } 0 \leqslant x - x_2 \leqslant 20\Delta x, \\ 0 & \text{otherwise.} \end{cases} \tag{18}$$

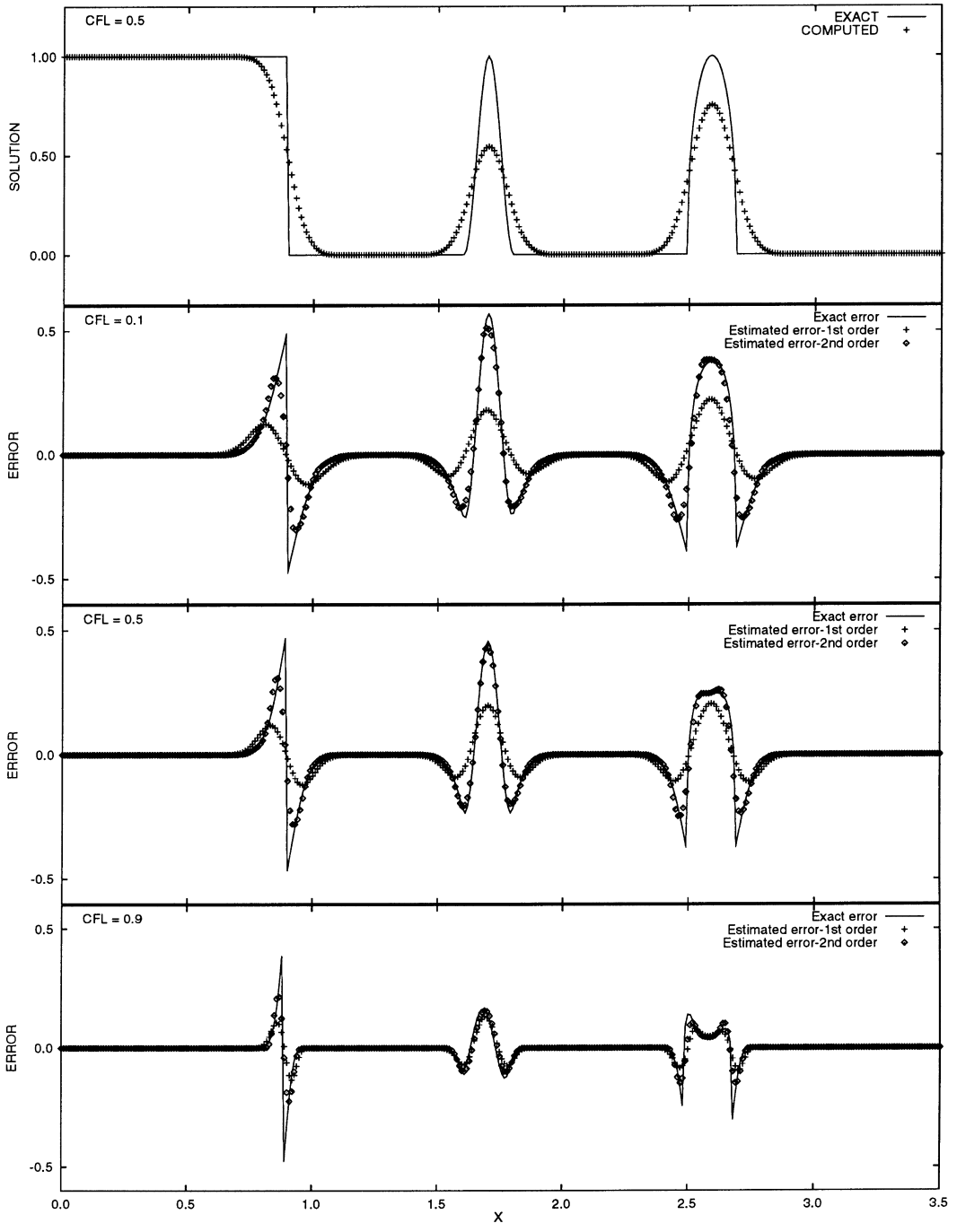

Fig. 1. Linear advection equation, $t = 0.8$.

The third profile is a semi-ellipse of width $20\Delta x$ which is initially centered at $x_3 = 1.4$:

$$\phi(x) = \begin{cases} \sqrt{1 - \dfrac{(x - x_3)^2}{(10\Delta x)^2}} & \text{for } |x - x_3| < 10\Delta x, \\ 0 & \text{otherwise.} \end{cases} \tag{19}$$

Fig. 1(a) shows a comparison of the computed solution profiles at a non-dimensional time of $t = 0.8$ using a CFL number $c = 0.5$, with the exact solution. The accuracy is poor due to the large numerical diffusion and will be worse with decreasing values of the CFL number and with increasing times. Solution of the proposed error equation are presented in Fig. 1(b), (c) and (d) for CFL numbers of $c = 0.1$, $c = 0.5$ and $c = 0.9$, respectively. Comparison with the exact error indicates that the location of the error is very well predicted by the error equation. The estimated error magnitudes using the first-order scheme are much lower than the exact ones, while the second-order results show remarkable agreement with the true error in all cases.

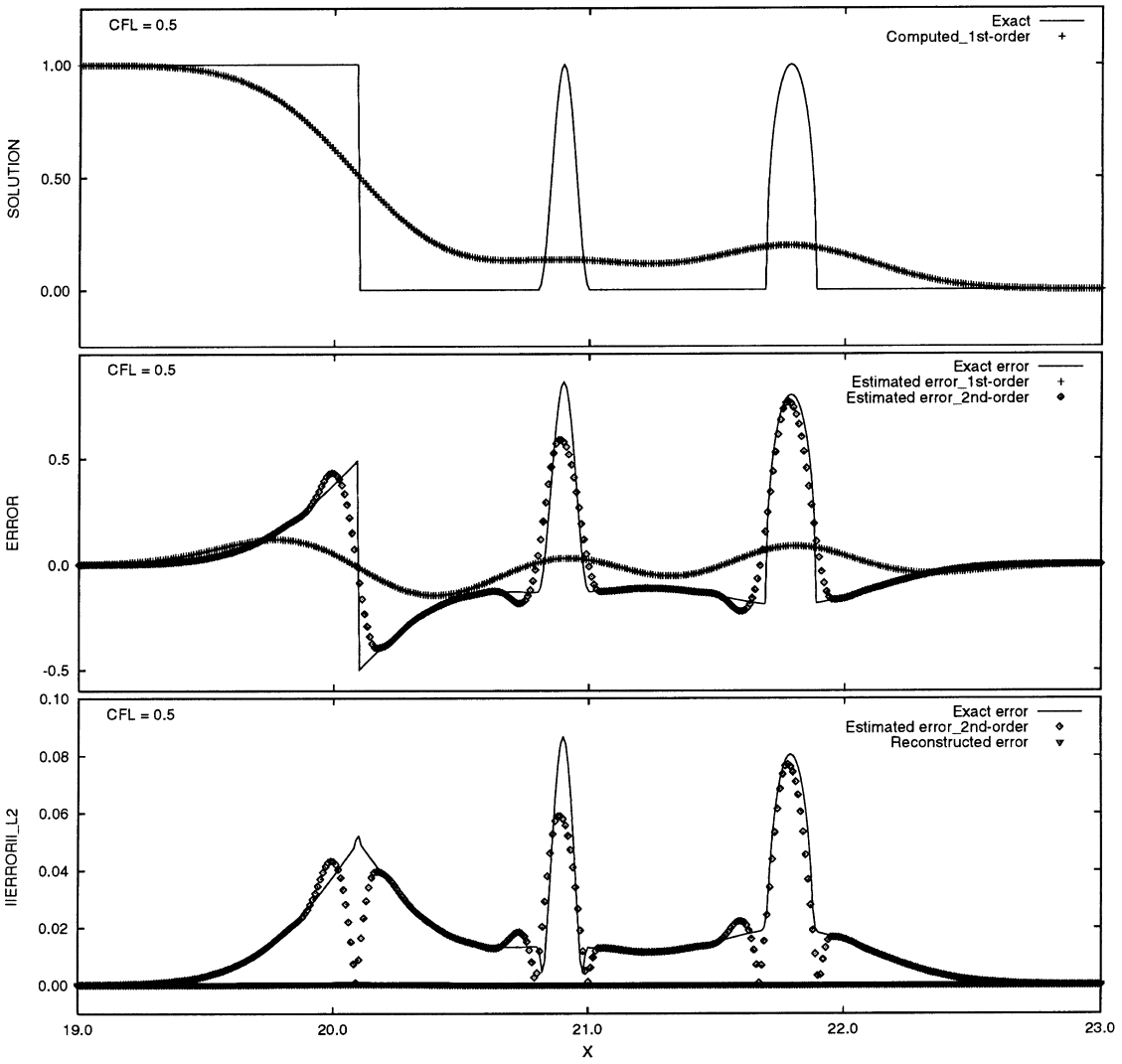

Fig. 2. Linear advection equation, $t = 20$.

Note that for $c = 0.9$, the difference in the error distributions between the first- and second-order schemes is not big, since the solutions themselves are much less diffused. If c is set to its maximum allowable value of one, both the first- and second-order schemes will reproduce the exact solution. In this case, zero error will be predicted as the error source will also be equal to zero.

When the computation is pursued for a longer time, the test profiles were further diffused and completely lost their shapes. Fig. 2(a) shows the solution at $t = 20$ in which the initial profiles can hardly be recognized. For such a diffused solution, most error estimators or indicators based on the local flow derivatives will fail

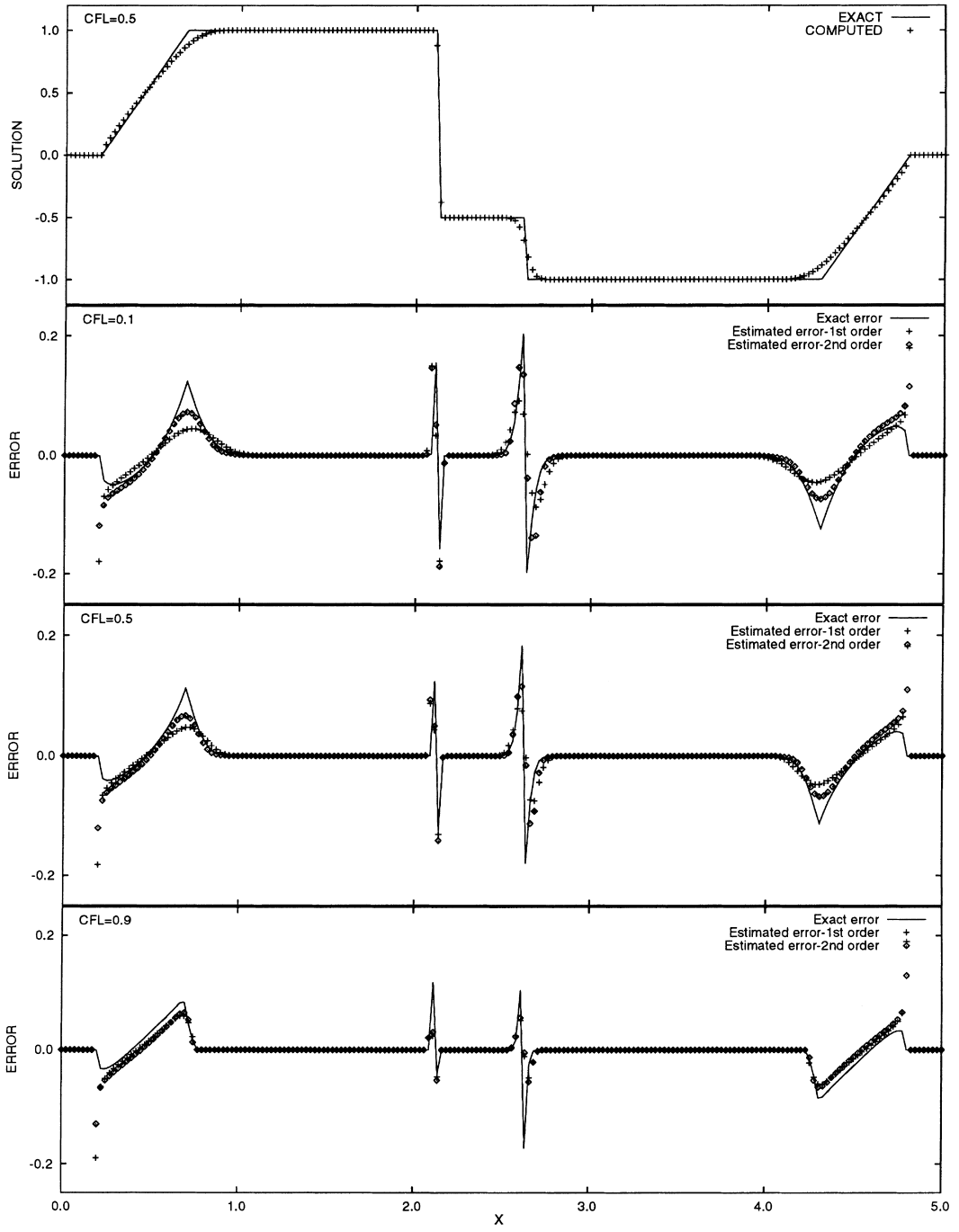

Fig. 3. Burgers' equation, $t = 0.5$, before any wave interaction.

to provide any useful error information. However, the present method combined with the second-order scheme captures the errors correctly as demonstrated in Fig. 2(b). For comparison, the L_2 norm of the estimated error using the local reconstruction technique (i.e. $\|\epsilon\|_{L_2} = \|u^* - u^h\|$ with u^* representing a higher-order reconstruction of the solution u^h, see for example Refs. [15,5]) is also plotted in Fig. 2(c) together with the corresponding exact and estimated errors using the present error estimator. The reconstruction technique works very poorly for this test case.

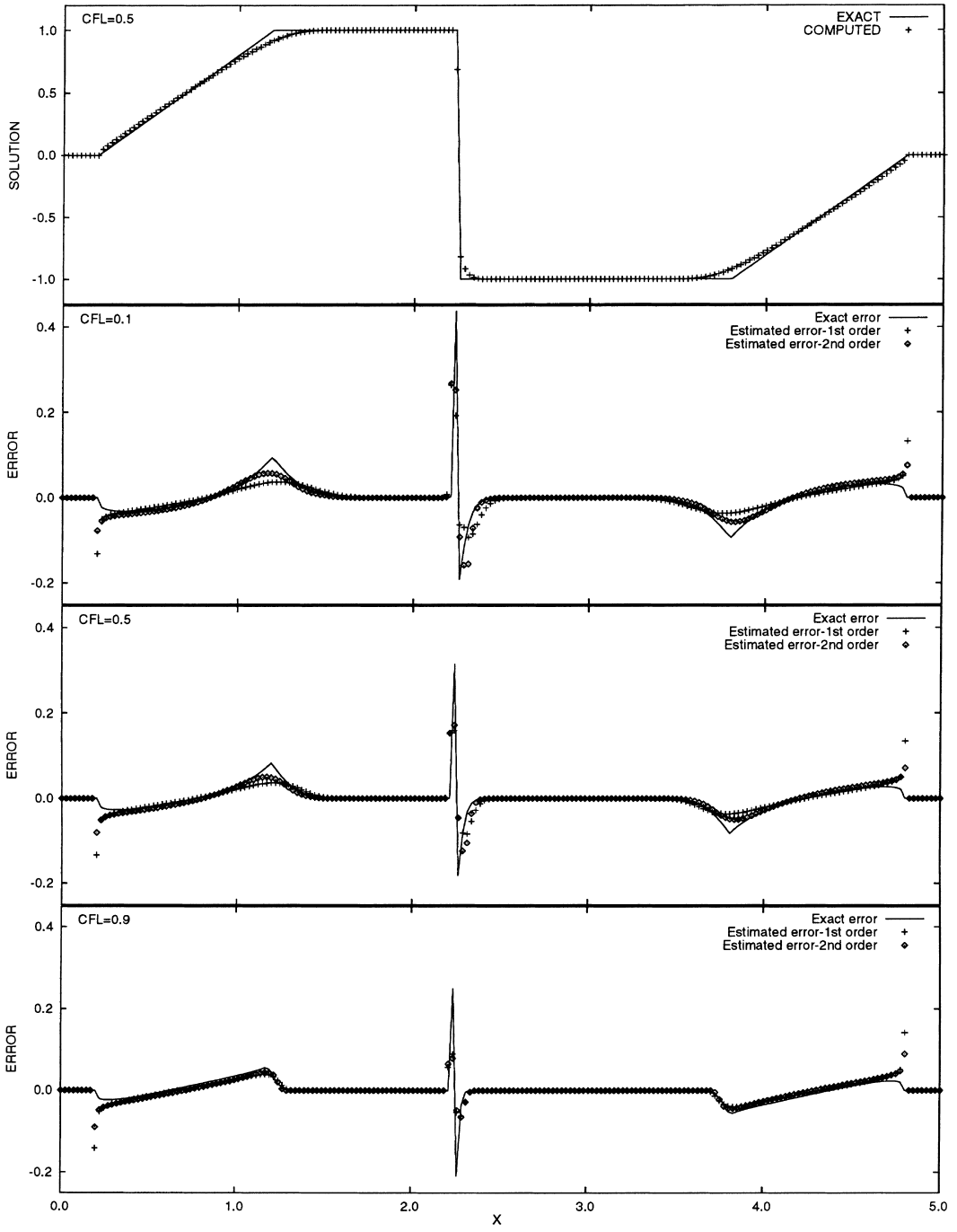

Fig. 4. Burgers' equation, $t = 1.0$, the two shocks collide and result in a steady shock.

5.2. Non-linear Burgers' equation

Burgers' equation is chosen to demonstrate the capability of the present error estimation technique for a non-linear equation. In this case, the flux function is $f(u) = u^2/2$ and the Jacobian is $A(u) = u$. The test case chosen is the IVP proposed by Yang and Przekwas [16] which presents discontinuity expansions and shock collisions. The initial profile is specified as

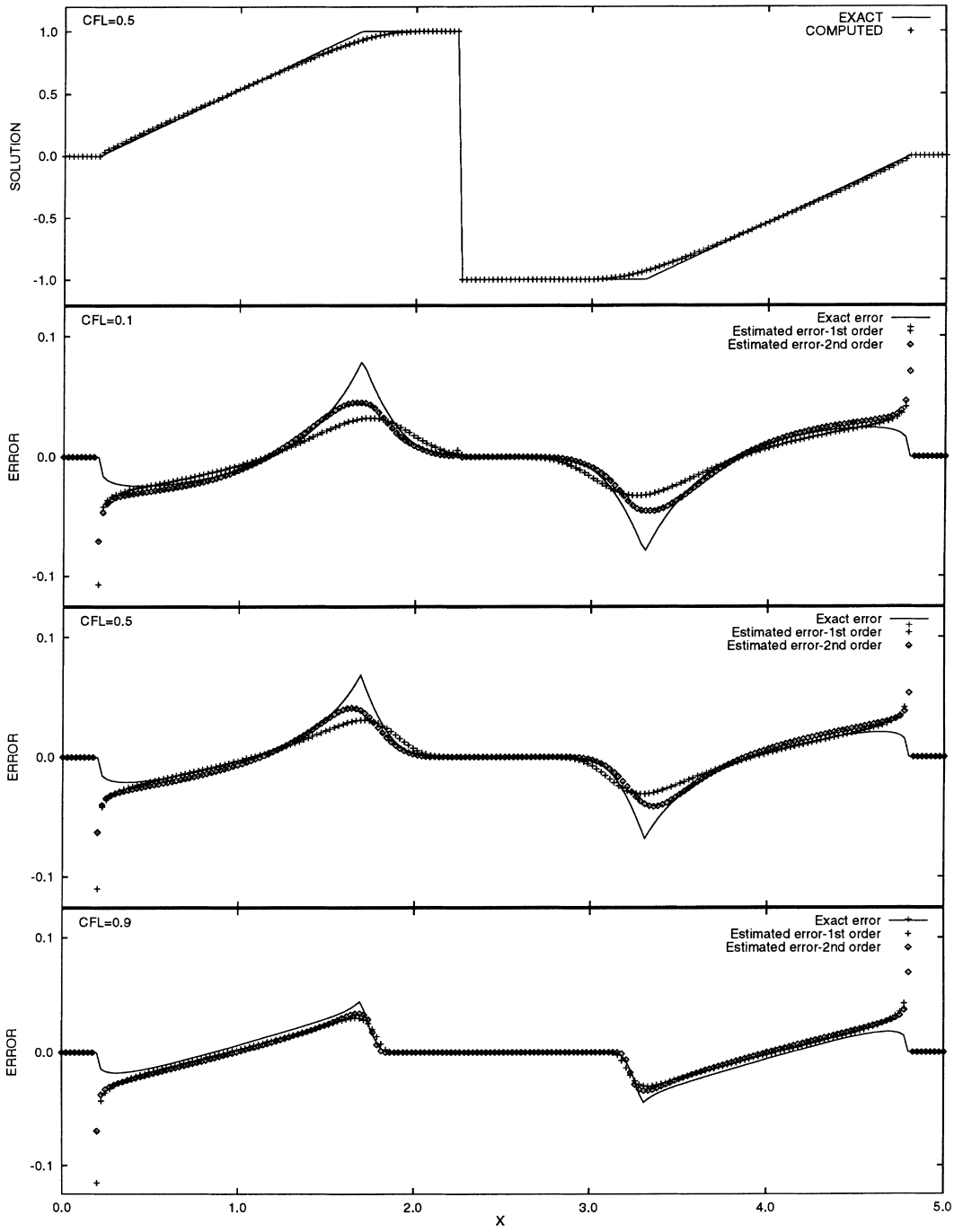

Fig. 5. Burgers' equation, $t = 1.5$, before the shock interacts with the two expansion waves.

$$\phi(x) = \begin{cases} 1.0 & \text{for } 0.2 < x < 2.0, \\ -0.5 & \text{for } 2.0 < x < 3.0, \\ -1.0 & \text{for } 3.0 < x < 4.8, \\ 0.0 & \text{otherwise.} \end{cases} \tag{20}$$

A uniform mesh is used with 200 cells within $[0, 5]$. The boundary points are not disturbed within the computational time period. The first-order solutions using $c = 0.5$ and the estimated error distributions

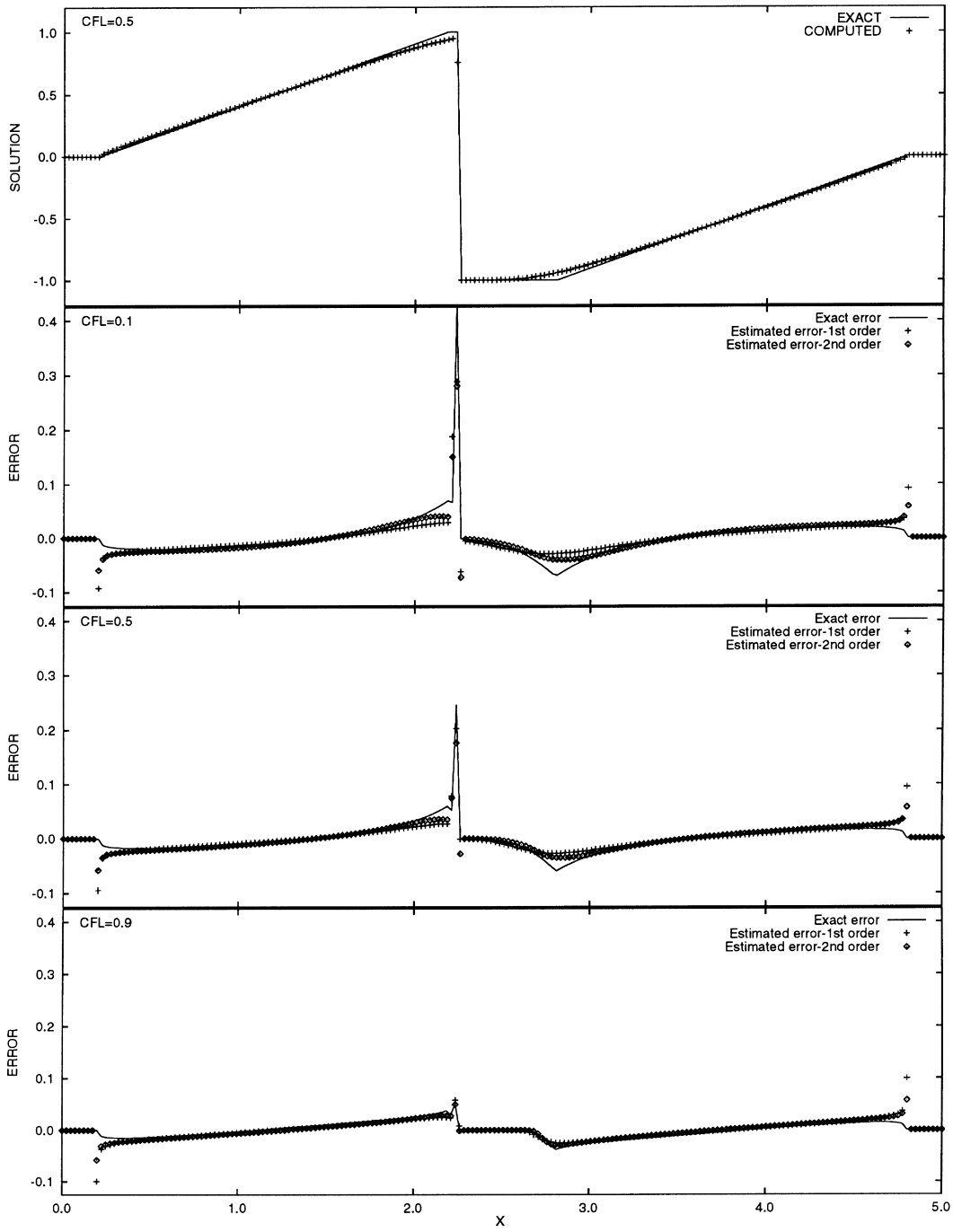

Fig. 6. Burgers' equation, $t = 2.0$, after interaction of the left expansion wave and the shock.

(both first- and second- order) are plotted in Figs. 3–6 with CFL numbers of $c = 0.1$, $c = 0.5$ and $c = 0.9$. Fig. 3 shows the solution comparisons at $t = 0.5$ before any wave interaction. Fig. 4 shows the results at $t = 1.0$, corresponding to the moment when the two shocks collide, which results in a stronger steady shock. After a while, the upwind scheme is able to capture the steady shock exactly since the steady shock location ($x = 2.25$) is at the grid cell interface, as shown in Fig. 5 at $t = 1.5$. It should be pointed out that if the steady shock position is not located at a cell interface, the shock cannot be resolved exactly and there will be one interior value between the left and the right values. For details, one can consult van Leer [17].

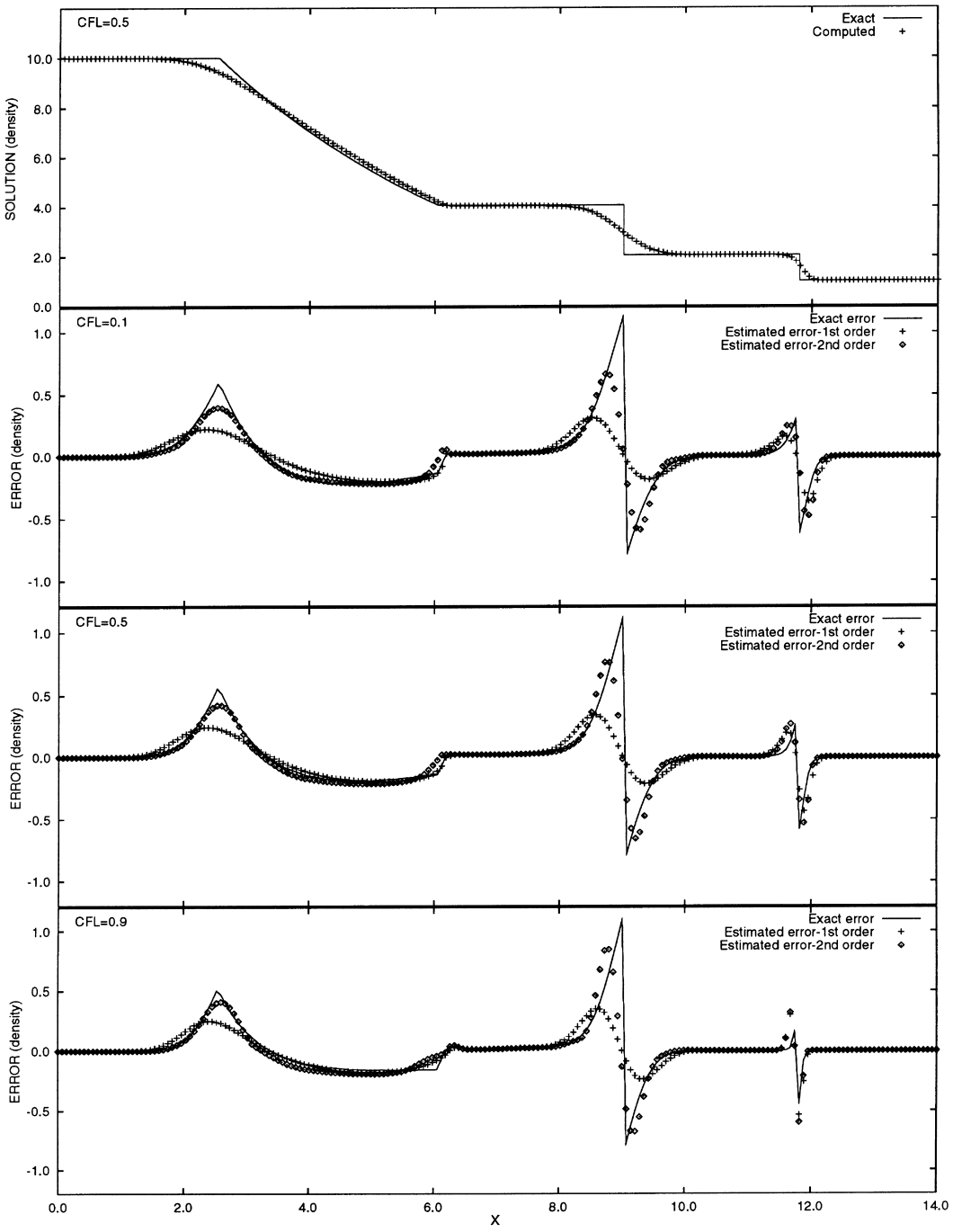

Fig. 7. Euler equations, $t = 3$, density distributions.

Finally, Fig. 6 shows the results at $t = 2.0$, after the interaction of the steady shock with the left expansion wave.

In the early stages of the simulation, the two shocks are propagated toward each other at different wave speeds. The faster (left) shock wave is less diffused than the slower (right) shock wave, and the two expansion waves behave anti-symmetrically, with more diffusion near the wave fronts (Fig. 3). For the diffused regions, the second-order scheme always provides better resolution for the error distributions. As in

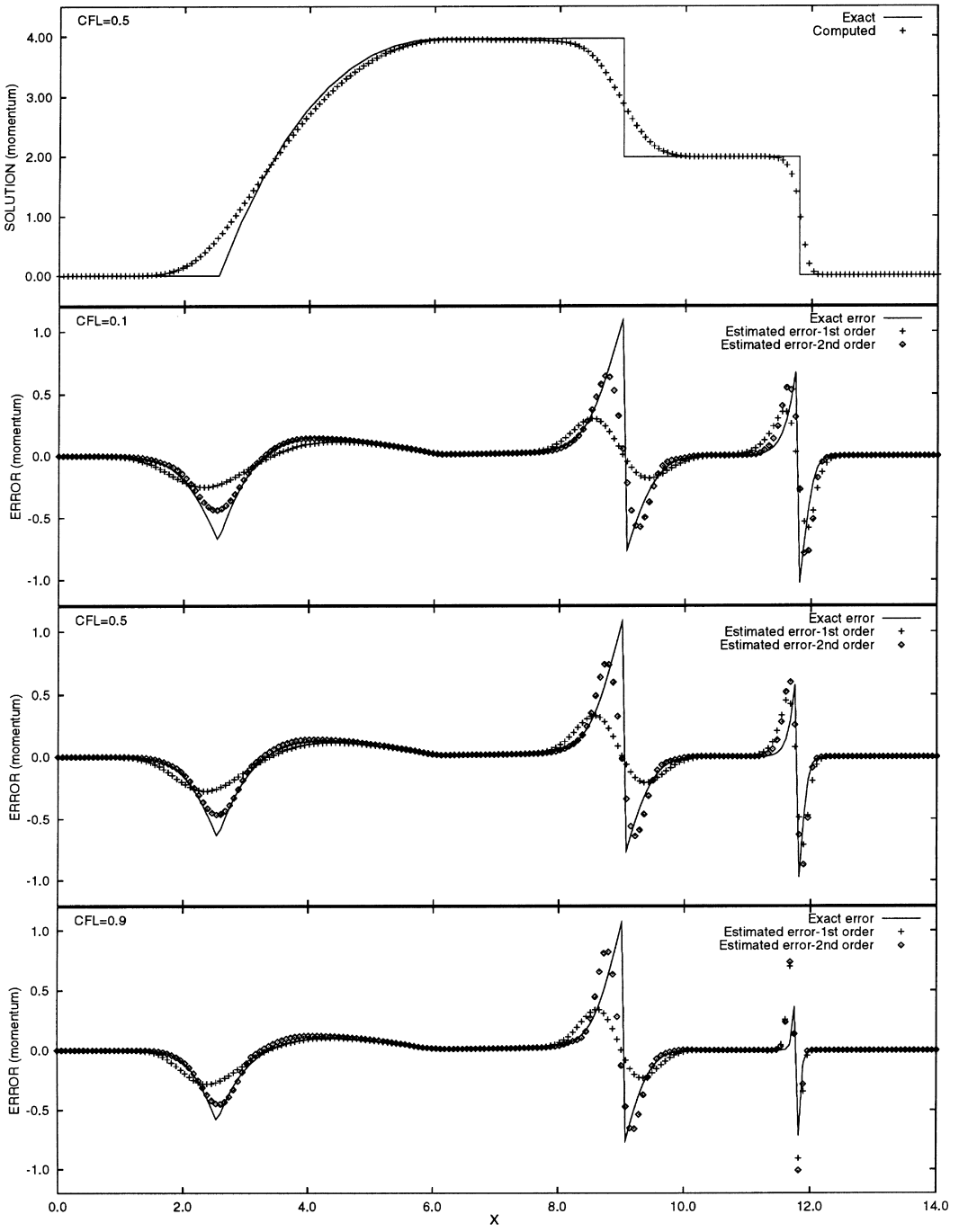

Fig. 8. Euler equations, $t = 3$, momentum distributions.

the linear case, when higher CFL numbers are used, the solutions are less diffused, and thus the differences between the first- and second-order solutions are smaller.

After the two shocks collide and form a stronger steady shock (Fig. 5), the present error estimator also produces no error across the shock, as the Roe scheme resolves this steady shock exactly on the present grid as mentioned before. This is one of the nice features of the proposed method and distinguishes it from many other error indicators and estimators based on solution derivatives, which generally would detect some error across a shock wave even if the shock had been resolved exactly.

When the steady shock interacts with the left expansion wave, the left side of the solution is diffused again. These errors are also captured correctly and at the proper location (Fig. 6).

5.3. Euler equations

The next test is for the non-linear Euler equations of gas dynamics. In the one-dimensional case, they represent the three conservation equations for mass, momentum and energy. The vectors of unknowns and flux are given by

$$u = \begin{pmatrix} \rho \\ \rho v \\ \rho e \end{pmatrix}, \quad f(u) = \begin{pmatrix} \rho v \\ \rho v^2 + p \\ \rho v e + v p \end{pmatrix},$$

where ρ is the density, v the fluid velocity, e the specific total energy and p the pressure. The system is closed by introducing the equation of state for a perfect gas:

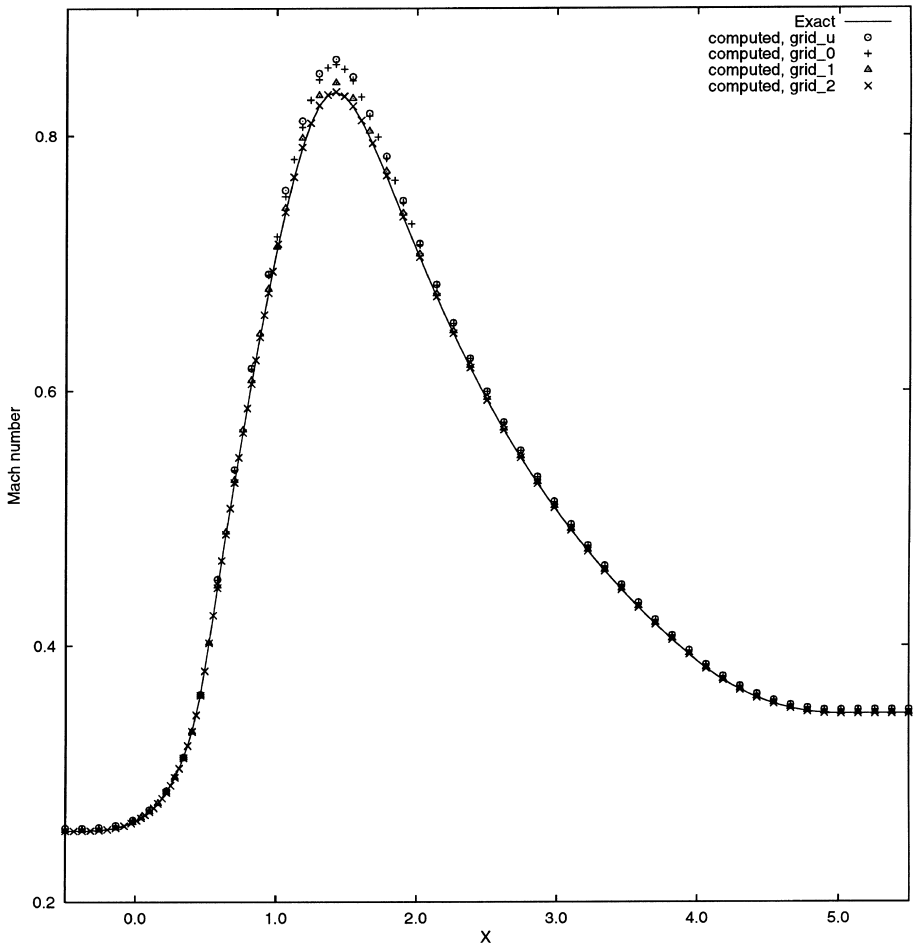

Fig. 9. Steady Euler equations, Mach number distributions using different grids.

$$p = \rho(\gamma - 1)\left(e - \frac{1}{2}v^2\right),$$

where, γ is the ratio of the specific heat capacities of the fluid.

The test case is an unsteady shock-tube IVP with a moving shock wave, an expansion wave and a contact discontinuity. The initial jump was positioned at $x = 6.1$ within the computational domain of [0, 14], with a density and pressure ratio of 10. The boundary points are not disturbed by the initial waves during the time period for the computation conducted in this paper. A uniform mesh of 200 cells is used.

Both the computed and exact solution profiles and error distributions at the non-dimensional time $t = 3.0$ are shown in Figs. 7 and 8 for the density and the momentum respectively. Again, the error distributions using CFL numbers of $c = 0.1$, $c = 0.5$ and $c = 0.9$ are presented for comparison. The error estimator for the Euler equations behaves similar to that of the scalar equation presented previously. The errors across the three different types of waves are well captured. The second-order solutions for the errors are less diffused than the first-order ones. However, unlike the scalar equation test cases, the influence of the CFL number from $c = 0.1$ to $c = 0.9$ is not as significant and the solution differences between the first- and second-order schemes are significant, even at $c = 0.9$. This can be attributed to the influence of local time step on solution accuracy and to the numerical diffusion of first-order upwind schemes [18]. In the scalar cases, the global CFL number of $c = 0.9$ corresponds to a time step very close to its maximum allowable

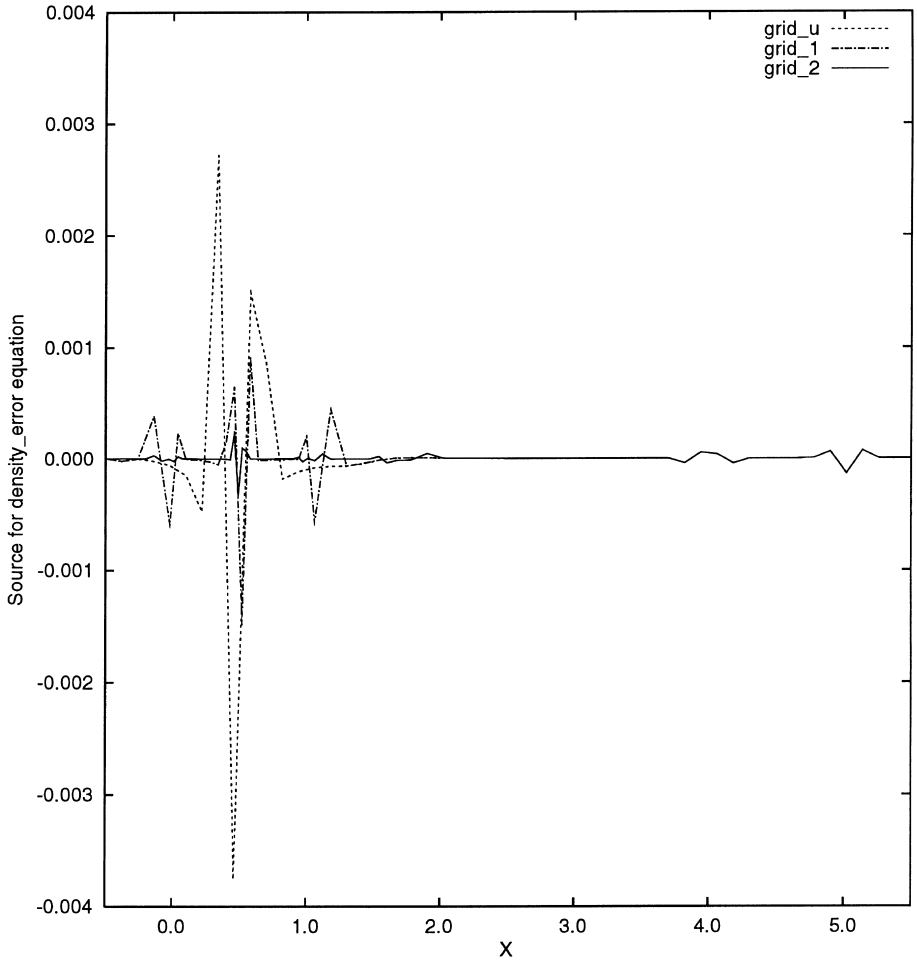

Fig. 10. Steady Euler equations, estimated error source distributions in the density error equation using different grids.

local time step; however, for a system of equations, the global CFL number of $c = 0.9$ is far from the allowable characteristic local time steps for the different waves [19]. As a result, at this CFL number, first-order results have poor resolutions across the contact discontinuity and the expansion wave. The space-time reconstructed second-order scheme [13] used here provides important improvement in the resolution of the error equations.

5.4. Steady Euler equations with variable cross-section

The last test concerns a steady BVP for the quasi-one-dimensional Euler equations representing compressible flow in a duct of variable cross-section. The equations can be written in the same form as Eq. (1) but with a source term

$$u_t + [f(u)]_x = s,$$

where

$$u = \mathscr{D}\begin{pmatrix} \rho \\ \rho v \\ \rho e \end{pmatrix}, \quad f(u) = \mathscr{D}\begin{pmatrix} \rho v \\ \rho v^2 + p \\ \rho v e + v p \end{pmatrix}, \quad s = \begin{pmatrix} 0 \\ p\frac{\partial \mathscr{D}}{\partial x} \\ 0 \end{pmatrix},$$

with $\mathscr{D} = \mathscr{D}(x)$ being the area function of the cross-section. A modified version of Roe's scheme [20] is used in the present computations to treat the source term s more accurately.

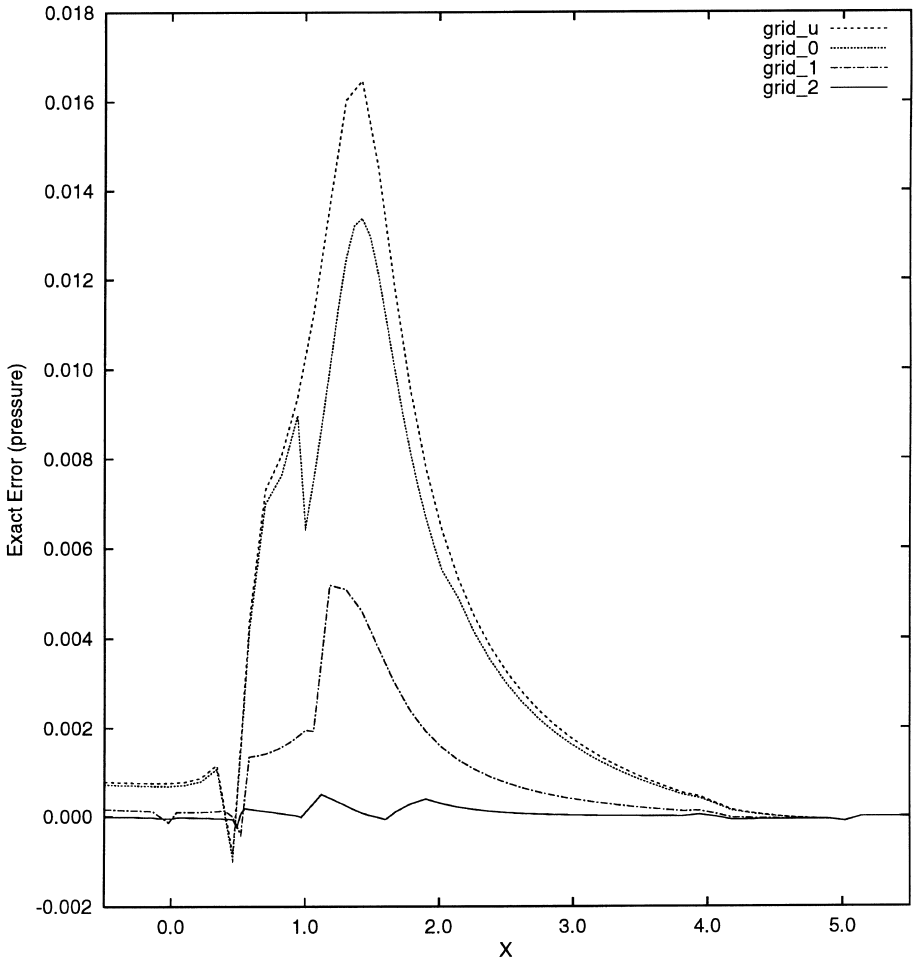

Fig. 11. Steady Euler equations, exact pressure error distributions using different grids.

The test case is conducted in an interval $[-0.5, 5.5]$ with area variation given by

$$\mathscr{D}(x) = \begin{cases} 3.25 - (x + 0.5)^{3.5} & \text{for } -0.5 < x \leqslant 0.5, \\ 0.5x + \frac{1}{x} & \text{for } 0.5 < x \leqslant 4.0, \\ 2.25 + \frac{7}{32}\left(1 + (x-5)^2\right) & \text{for } 4.0 < x \leqslant 5.0, \\ 2.25 + \frac{7}{32} & \text{for } 5.0 < x. \end{cases}$$

Subsonic flow is considered. At the inlet, pressure is extrapolated from the first cell value and the other variables are computed using isentropic flow condition with $p_0 = 1$ and $T_0 = 1$. At the outflow boundary, pressure is imposed as $p_{ex}/p_0 = 0.92$ and the velocity and the temperature are extrapolated from the last cell.

The first computation is conducted using a uniform grid with 50 cells (*grid_u*) and a CFL number of 0.85. Fig. 9 shows the computed Mach number distribution compared with the analytical solution. The estimated error source $-r(u^h)$ for the density-equation, the exact error in pressure and the exact and estimated errors in density are plotted in Figs. 10–12(a), respectively. The qualitative distribution of the estimated density error resembles the true error distribution.

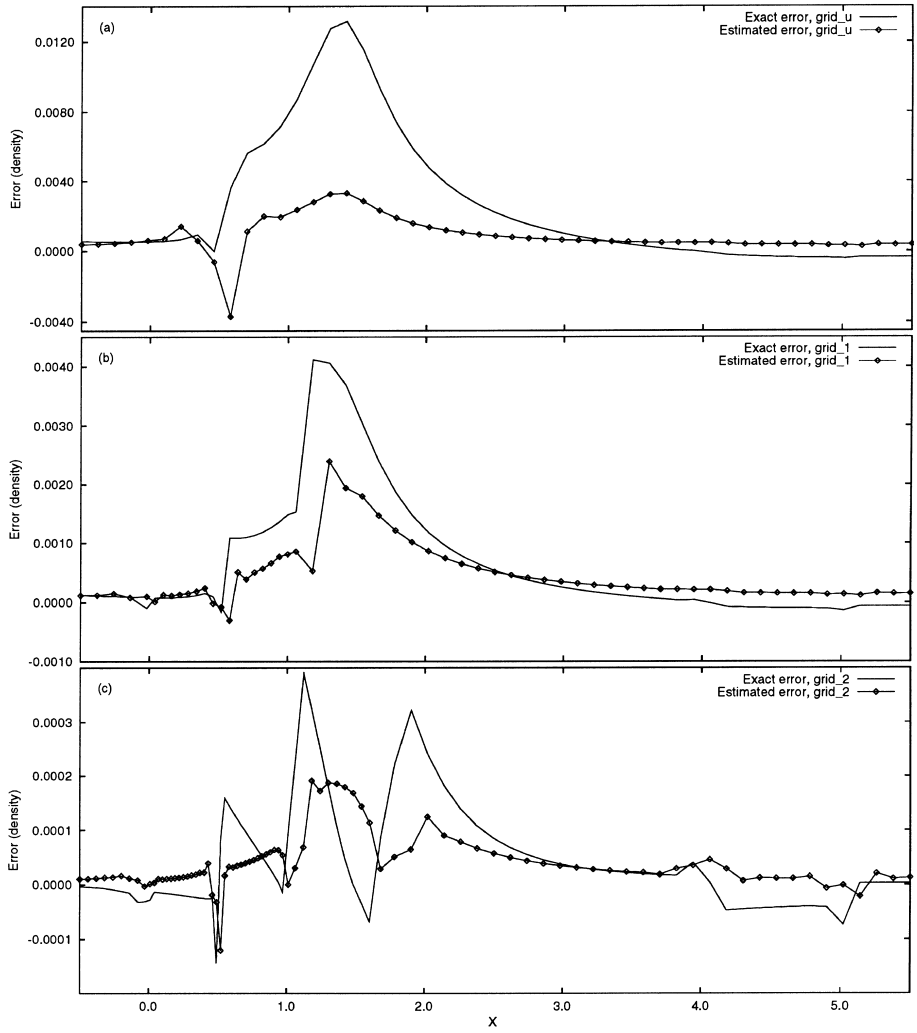

Fig. 12. Steady Euler equations, exact and estimated density error distributions using different grids.

5.4.1. Grid adaptation experiments

Most grid adaptation strategies try to equidistribute the error in the computational domain. From Figs. 10–12(a), it is clear that the solution error is maximum within the interval $[1.0, 2.0]$ while the error source is maximum between 0.0 and 1.0. In a first test, the adapted grid named *grid*_0 is obtained by refining grid *grid_u* by a factor of two within the interval $[1.0, 2.0]$, where the error is maximum. This results in a non-uniform grid with 59 cells. This leads to little solution improvement as shown in Figs. 9 and 11. A second adapted mesh, *grid*_1 is obtained by refining grid *grid_u* by a factor of two in the region where the error sources are dominant, i.e. within the interval $[0.0, 1.0]$. This also results in a 59 cells grid. On *grid*_1, the computed solutions are much improved as illustrated in Figs. 9 and 11. This is an example of the non-local nature of the error and its estimation process for hyperbolic conservation laws. This adaptation process can be further pursued based on the estimated density error source (Fig. 10) for *grid*_1. The mesh is thus further refined (cut by two) within the interval $[-0.5, 1.7]$, leading to a grid of 85 cells (*grid*_2). The solution on *grid*_2 now agrees very well with the analytical solution (Fig. 9), the error sources are equidistributed (Fig. 10) and the exact errors are decreased drastically (Fig. 11). The estimated density errors for *grid_u*, *grid*_1 and *grid*_2 presented in Fig. 12(a), (b) and (c) show how the estimated error approaches the exact error as the grid is refined. This test problem illustrates that an efficient grid adaptation can be achieved using the estimated error source instead of the error distribution itself.

6. Concluding remarks

An a posteriori error estimation technique has been proposed for hyperbolic conservation laws. The method is based on the solution of a linearized hyperbolic equation with source term for the error. The error source is approximated using the modified equation approach.

Many useful features of this technique have been demonstrated for one-dimensional unsteady and steady test cases. First, in all the test problems, the estimated errors are a good approximation of the true errors in terms of both their locations and their magnitudes. This is especially true when a second-order scheme is used to solve the error equations. Second, the proposed error equation together with the estimated error source can track waves and capture the erroneous waves globally and correctly. Third, the estimated error source term may be used as an indicator for grid adaptation, as demonstrated in the last test case.

Although the numerical experiments were conducted using Roe's upwind scheme, other upwind finite-volume schemes can be applied to the error equations and to the error source approximation.

Acknowledgements

The authors would like to express their appreciation to Dominique Pelletier of École Polytechnique de Montréal and Paul Labbé of CERCA for several helpful discussions and suggestions. Thanks also go to the reviewers for their useful comments and suggestions to improve the paper. The financial support provided by the Natural Science and Engineering Research Council (NSERC) of Canada and the Centre de Recherche en Calcul Appliqué (CERCA) is gratefully acknowledged.

References

[1] K.W. Mortan, E. Süli, A posteriori and a priori error analysis of finite volume methods, in: J.R. Whiteman (Ed.), The Mathematics of Finite Elements and Applications, Ch. 18, Wiley, New York, 1994.

[2] M. Reggio, J.Y. Trépanier, H. Zhang, R. Camarero, Numerical simulation of the gas flow in a circuit-breaker, Int. J. Numer. Meth. Engrg. 34 (1992) 607–618.

[3] B. Palmério, A. Dervieux, 2D and 3D unstructured mesh adaption relying on physical analogy, in: Proceedings of the Second International Conference on Numerical Grid Generation in CFD, Barcelona, 1988, pp. 178–185.

[4] H. Paillére, K.G. Powell, D.L. De Zeeuw, A wave-model-based refinement criterion for adaptive-grid computations of compressible flows, In AIAA Paper 92-0322, 1992.

[5] A. Ilinca, R. Camarero, J.-Y. Trépanier, M. Reggio, Error estimator and adaptive moving grids for finite volume schemes, AIAA J. 33 (11) (1995) 2058–2065.
[6] T. Sonar, E. Süli, A dual graph-norm refinement indicator for finite volume approximations of the Euler equations, Numerische Mathematik 78 (4) (1998) 619–658.
[7] B.P. Van Straalen, R.B. Simpson, G.D. Stubley, A posteriori error estimation for finite volume simulations of fluid flow transport, in: Proceedings of the Third Annual Conference of CFD Society Canada (CFD95) 25–27 June 1995, Banff, Alberta.
[8] B. Szabó, I. Babuška, Finite Element Analysis, Wiley, New York, 1991.
[9] D. Pelletier, A. Zali, A. Fortin, Adaptive remeshing for hyperbolic transport problems, Int. J. Comp. Fluid Dyn. 3 (1994) 79–99.
[10] G.H. Klopfer, D.S. McRae, Nonlinear truncation error analysis of finite difference schemes for the Euler equations, AIAA J. 21 (4) (1983) 487–494.
[11] K.A. Hoffmann, Computational fluid dynamics for engineers, Engineering Education System, Austin, Texas, USA, 1989.
[12] P.L. Roe, Approximate Riemann solvers, parameter vectors, and difference schemes, J. Comput. Phys. 43 (2) (1981) 357–372.
[13] X.D. Zhang, J.-Y. Trépanier, R. Camarero, A space-time reconstruction algorithm for steady and unsteady Euler equations, in: The AIAA 34th Aerospace Science Meeting & Exhibit, 1996. AIAA Paper 96-0529, 6–10 January, Reno, USA.
[14] B.P. Leonard, The ULTIMATE conservative difference scheme applied to unsteady one-dimensional advetion, Computer Meth. Appl. Mech. Engrg. 88 (1991) 17–74.
[15] J.A. Peraire, M. Vahdati, K. Morgan, O.C. Zienkiewicz, Adaptive remeshing for compressible flow computations, J. Comput. Phys. 72 (1987) 449–466.
[16] H.Q. Yang, A.J. Przekwas, A comparative study of advanced shock-capturing schemes applied to Burgers' equation, J. Compt. Phys. 102 (1992) 139–159.
[17] B. van Leer, On the relation between the upwind-differencing schemes of Godunov Engquist–Osher and Roe, SIAM J. Sci. Stat. Comput. 5 (1) (1984) 1–20.
[18] X.D. Zhang, J.-Y. Trépanier, M. Reggio, R. Camarero, A time-accurate local time stepping method based on a flux-updating procedure, AIAA J. 32 (9) (1994) 1926–1929.
[19] W.-T. Lee, Local preconditioning of the Euler equations, PhD thesis, The University of Michigan, 1992.
[20] P.L. Roe, Characteristic-based schemes for the Euler equations, Ann. Rev. Fluid Mech. 18 (1986) 337–365.